Electronic Supplementary Material (ESI) for Journal of Materials Chemistry A.

Supporting Information

Less is More: Tiny Amount of Insoluble Multi-Functional Nanoporous Additive Plays a Big Role in Lithium Secondary Battery

Ruoxuan Qi[a,b], Chao Yang[c], Liujia Ma[b], Xiaoying Fan[b], Qiaoyun Wu[b], Chao Wang[d], Ya-Jun Cheng[*b], Kunkun Guo[*c], Yanfeng Gao[a], Yonggao Xia[*b,e]

Experimental Section

Materials: 5,5′,6,6′-Tetrahydroxy-3,3,3′3′-tetramethyl-1,1′-spirobisindane (TTSBI) were purchased from Alfa Aesar. 2,3,5,6-Tetraflfluoroterephthalonitrile (TFTPN) was obtained from Sigma-Aldrich (USA). N, N-Dimethylformamide (DMF) and methanol were acquired from SCR (China). K_2CO_3 was purchased from Macklin (China). Poly (vinylidene fluoride) (PVDF) was donated by Solvay. N-Methyl-2-pyrrolidone (NMP) and dimethyl sulfoxide (DMSO) were purchased from Aladdin Reagent Co., Ltd., China. Conductive carbon black (Super P) was acquired from SCM Chem. Shanghai, China. The electrolyte composed of 1 M of $LiPF_6$ in ethylene carbonate (EC)/ dimethyl carbonate (DMC) (3:7 in volume) was purchased from Mitsui Chemicals Co., Ltd. (China). Carbon coating aluminum foils with the thickness of 16 μm were obtained from SCI Materials Hub Co., Ltd. (China).

Synthesis of PIM-1: The reaction procedure of PIM-1 is shown in **Figure 1**. The synthesis of PIM-1 was carried out with slight modification from the previously reported work. PIM-1 was synthesized through a condensation reaction between TTSBI (3.404 g) and TFTPN (2.001 g) monomers at 68 ℃ for 48h in anhydrous DMF (70 mL) assisted by dissolved anhydrous K_2CO_3 (2.820 g). Then, the product was washed by methanol for three times and further dried in the oven at 120 ℃ overnight.[1, 2]

Characterization of PIM-1: Molecular structure of PIM-1 was characterized by ^1H NMR (AVANCE 400 MHz, Bruker, Switzerland) with $CDCl_3$ as the solvent and Fourier transform infrared (FTIR) spectra (Cary660+620, Agilent, American). The wavenumber range of the FTIR spectra was from 1000 cm^{-1} to 4000 cm^{-1}. The

molecular weight of as-synthesized PIM-1 was measured by gel permeation chromatography (HLC 8320, TOSOH, Japan) (polystyrene standard in tetrahydrofuran (THF)) to give a number-average molecular weight of around 7500 g·mol^{-1}. Thermal stability of the synthesized PIM-1 was measured by a thermogravimetric analyzer (TGA 8000-Spectrum two-Clatus SQ8T, PerkinElmer, American) with the temperature range from 30 °C to 800 °C at a heating rate of 10 °C min^{-1} under N_2 atmosphere. The specific surface area and the porosity measurement were carried out based on N_2 adsorption−desorption test by using the Brunauer-Emmett-Teller (BET) method with a Micromeritics ASAP2020HD88 accelerated surface area and Porosimetry system. Before the measurements, the PIM-1 sample (116 mg) was degassed under reduced pressure (<1022 Pa) at 150 °C for 12 h. Corresponding pore-size distribution data was derived from the N_2 sorption isotherms at 77 K based on Barrett-Joyner-Halenda (BJH) model. The resistivity measurement was carried out on Physical Property Measurement System (PPMS-EverCool, QD, USA) with a temperature range from 100 K to 300 K. The test current was 0.1 mA, and the frequency was 60 Hz. Silver paste (H20E silver epoxy) used for connecting platinum wires was obtained from EPO-TEK Co., Ltd. The sample preparation procedure was as following. First, 10 mg, 5 mg, 1 mg, and 0 mg of the PIM-1 additive or PVDF binder was separately mixed with 100 mg of conductive carbon black (Super P) and dispersed in sufficient THF solvent by stirring for 4 h. The mixture was then dried at 80 °C in an air circuiting oven, which were then ground into fine powder in a mortar. Thereafter, 5 mg of the mixture powder was pressed into a mould with the size of 7 mm × 3 mm using an infrared press machine with a pressure

of 20 MPa. TEM experiment was performed with a JEOL2100-JEM2100 TEM instrument from Japan operated at 200 kV. The TEM samples were prepared by dissolving 10 mg of PIM-1 or PVDF in THF and NMP respectively and further mixed with 100 mg of Super P, followed by drying at 80 °C in air-circuiting oven for 8 h.

Fabrication of $LiNi_{0.8}Co_{0.1}Mn_{0.1}O_2$ (NCM811) Cathode and Assembly of NCM811‖Li half-cell: The NCM811 cathodes were fabricated with either PIM-1 or PVDF (NCM/PIM and NCM/PVDF) via a slurry coating procedure. The mass compositions of the electrodes regarding the NCM811, Super-P and PIM-1/PVDF were varied as 89:10:1, 89.5:10:0.5, 89.9:10:0.1 respectively. DMSO was used as a dispersion medium to fabricate the NCM/PIM electrodes with the PIM content of 1.0%, 0.5%, 0.1%, and 0.05%. Because PIM-1 is insoluble in DMSO, DMSO was mainly used as dispersion medium to form a homogeneous slurry for further casting. NMP was used as a solvent to dissolve PVDF and further dispersion medium to disperse NCM811 and super P particles. The slurry was cast on the carbon coating aluminum foil, followed by drying at 80 °C overnight to remove the solvent. After the electrodes were dried and pressed, they were cut into identical round electrodes with a diameter of 14 mm. The mass loading of the active material was controlled at a range from 3.72 to 5.42 $mg \cdot cm^{-2}$. The actual mass loading densities with respect to the active material are listed in Table S3. The coin-type cells were assembled in a glove box (MBRAUN UniLab) with oxygen and water levels of less than 0.1 ppm. Lithium metal was used as a counter electrode and a polypropylene microporous film (Celgard 2300) was used as a

separator. The electrolyte was composed of 1 M $LiPF_6$ dissolved in EC and DMC (3:7 in volume).

Electrochemical Tests and Structural Characterization of the NCM/PIM and NCM/PVDF Electrodes: All cycling and rate tests were conducted with a voltage range from 2.8 V to 4.3 V at room temperature on a Land Battery Test System. And the rate performance tests were carried out with a current density range from 0.1 C to 5 C and further at 1 C (1 C=200 $mAh.g^{-1}$). Cyclic voltammetry measurements (2.8 V - 4.3 V) and electrochemical impedance spectroscopy tests (0.01 Hz to 1 MHz, 10 mV) were performed on an electrochemical workstation (Solartron Analytical). Scanning electron microscopy (SEM) was displayed by a Hitachi S4800 cold-field emission scanning electron microscope equipped with an energy-dispersive X-ray spectrometer (EDS). X-ray photoelectron spectroscopy (XPS) measurements were carried out using an Axis Ultra DLD XPS spectrometer. The XPS samples were prepared by disassembling the cycled cells in a glove box after 100 cycles at 0.2 C, followed by washing with DMC for three times to remove residual electrolyte at the electrode surface and further dried for 1 h in the glove box.

Fabrication of $LiNi_{0.5}Co_{0.2}Mn_{0.3}O_2$ (NCM523), $LiFePO_4$ (LFP), $LiCoO_2$ (LCO) Cathodes, Assembly and Electrochemical Tests of NCM523‖Li, LFP‖Li, and LCO‖Li Half-cells: The NCM523, LFP, LCO cathodes were fabricated with either PIM-1 or PVDF via a slurry coating procedure similar to the NCM811‖Li half-cell except the mass compositions. In details, the mass compositions of the NCM523/PIM and NCM523/PVDF electrodes regarding the NCM523, Super-P and PIM-1/PVDF

were varied as 89:10:1. Also, the ratios of LFP/ (PIM or PVDF) and LCO/ (PIM or PVDF) cathodes were maintained as 89:10:1 and 89.5:10:0.5. The electrochemical performance tests were performed with similar protocol to the NCM811‖Li.

Calculation Methods:

Structure Optimization: All structures were optimized using the density functional theory (DFT) with the B3LYP functional and 6-311+G (d, p) basis set by Gaussian 09 software. Grimme's DFT-D3 correction was used in the structural optimization process.[3] The conductor-variant polarized continuum model (CPCM)[4] was employed to carefully reflect the influence of dielectric medium on the molecular geometric. In principle, this is useful for describing the interaction between a highly Li^+ and PF_6^- ion and molecular in a polar medium. We adopted a dielectric constant of 29.1, which corresponds to the weight-averaged value for EC (89.78): DMC (3.11) = 3:7 volume ratio medium. All of the molecular energy was calculated using the density functional theory (DFT) with the B3LYP functional and def2tzvp basis set. The adsorption energy (Ead) is calculated using the formula:

$$E_{ad} = E_{total} - E_{molecular} - E_n \quad (1)$$

Where E_{total} is the total energy of Li^+, PF_6^- and LiF absorbed on the molecular, $E_{molecular}$ is the total energy of molecular, E_n is the total energy of Li^+, PF_6^- and LiF. The electrostatic potential and charge density difference was visualized in collaboration with Multiwfn[5] and VMD[6].

Molecular dynamics simulation: The molecular configuration of PIM was studied by molecular dynamics (MD) simulation. MD simulations adopted Forcite module in the

Materials Studio software using COMPASS force field.[7] Initial configurations of PIM were created by putting 10 PIM polymer chains and 300 dimethyl sulfoxide (DMSO) molecules randomly in the simulation box and setting the initial density as 1.0 $g \cdot cm^{-3}$. Each polymer chain has 5 monomers and 300 DMSOs were added for the purpose of simulating the real situation. After geometric optimization, the configurations of the molecules in the simulation box with the lowest energy were selected. Then, to achieve the thermodynamic equilibrium of such a box at ambient temperature and pressure, the simulated system was firstly applied under constant temperature and constant volume (NVT ensemble) at 400 K for 2000 ps, and then further applied to a series of NPT simulations, each of which lasted for 200 ps of simulation time. The NPT simulations were performed step-by-step in the following order: 350 K-100 MPa, 350 K-10 MPa, 350 K-1 MPa and 298 K-0.1 MPa.[8]

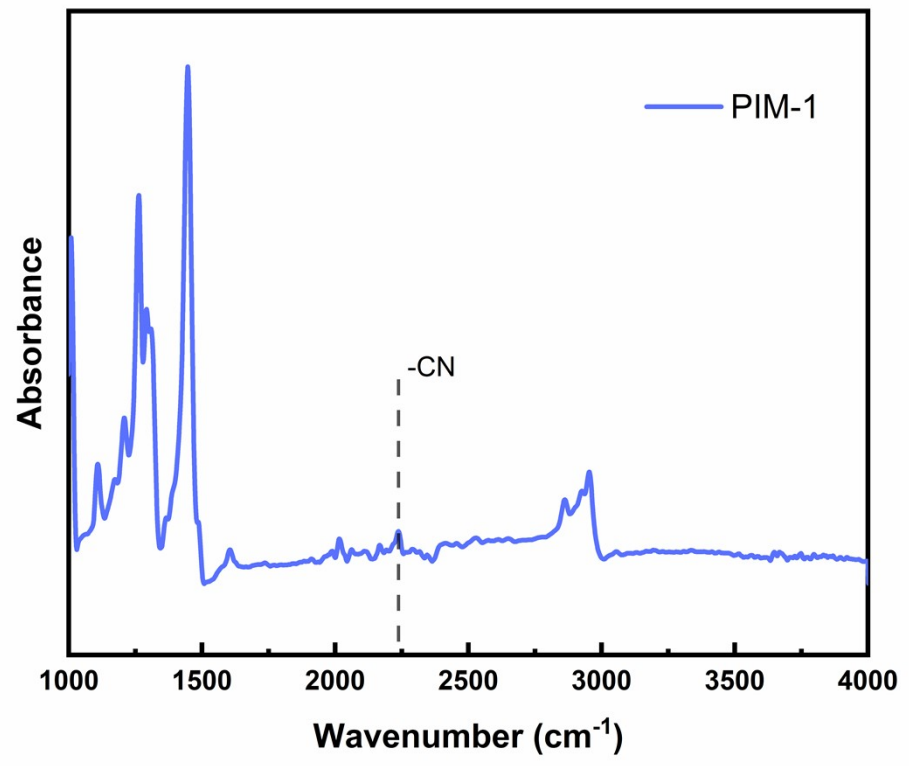

Figure S1. FTIR spectra of PIM-1.

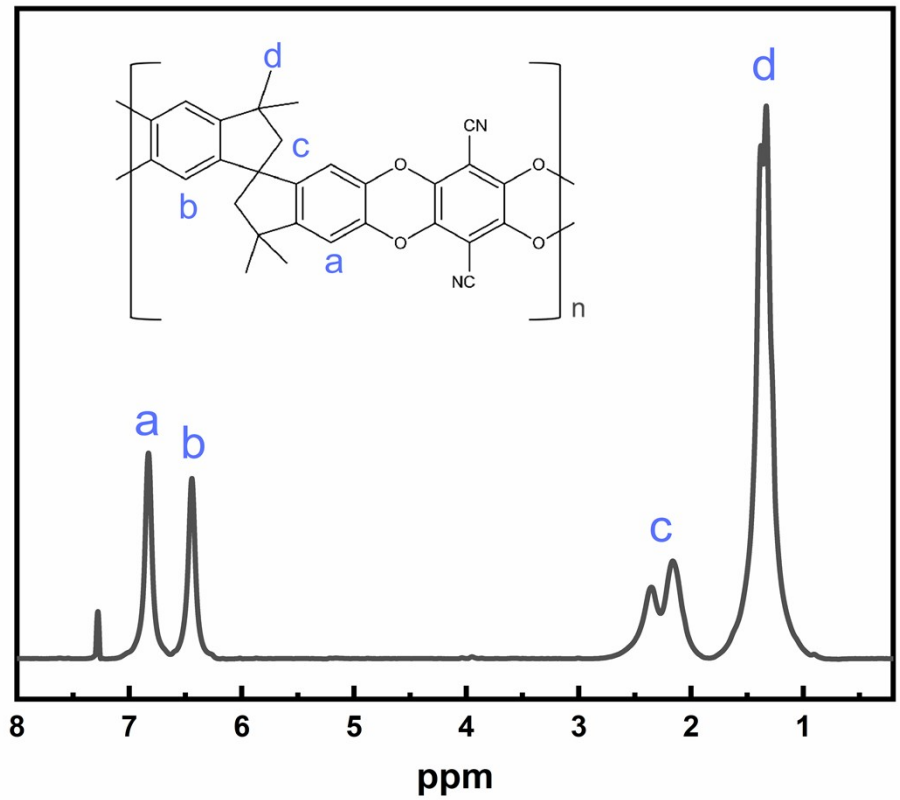

Figure S2. ^{1}H NMR spectroscopy of PIM-1.

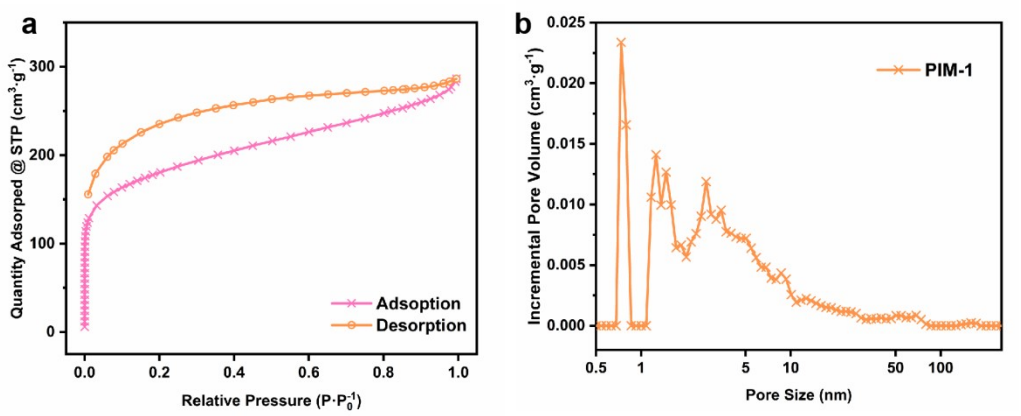

Figure S3. N_2 adsorption/desorption isotherm (a) and pore size distribution profile (b) of PIM-1.

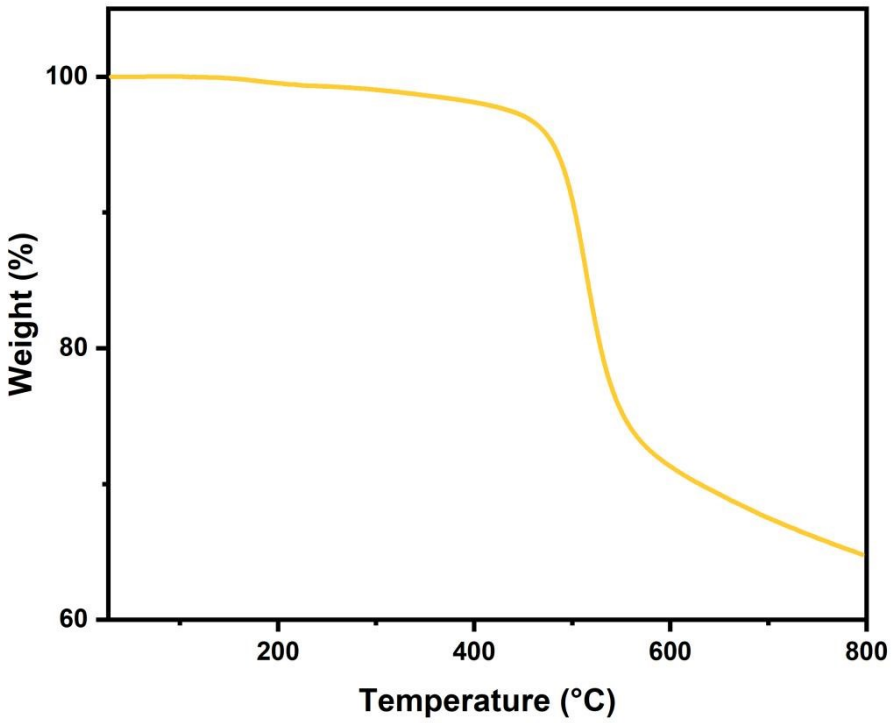

Figure S4. TGA thermogram for synthesized PIM-1.

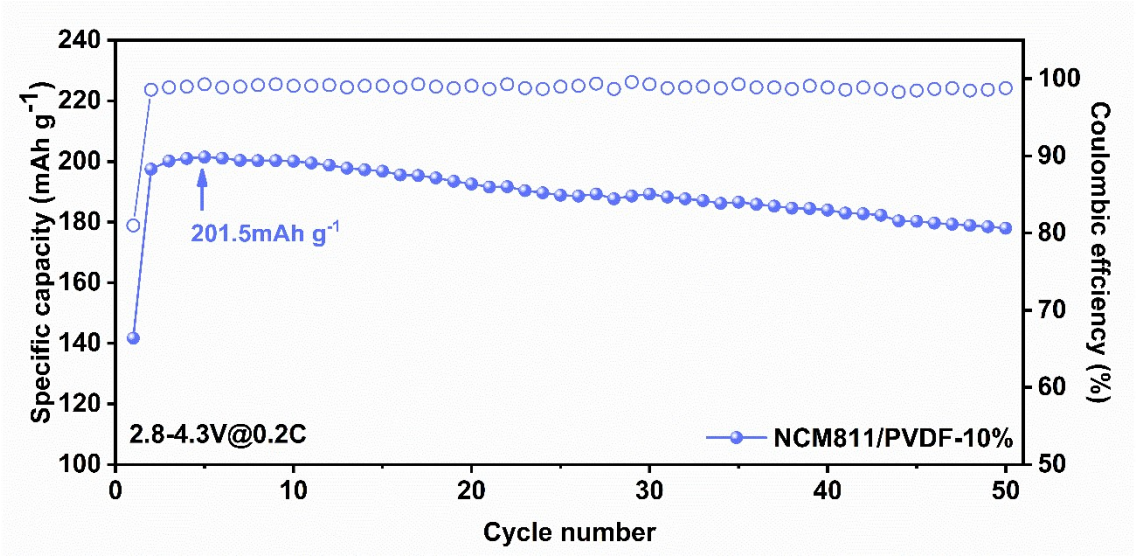

Figure S5. Cyclic performance in terms of discharge capacity and coulombic efficiency of the NCM811/PVDF-10% electrode with the voltage between 2.8 V and 4.3 V at 0.2 C (1C=200 $mA{\cdot}g^{-1}$) in the electrolyte of 1 M $LiPF_6$ in EC/DMC (vol ratio of EC:DMC=3:7).

Table S1. Rate performance of the NCM/PIM and NCM/PVDF electrodes with different mass compositions of PIM and PVDF.

Rate/Capacity ($mAh \cdot g^{-1}$)	0.1 C	0.2 C	0.5 C	1.0 C	2.0 C	5.0 C	1.0 C
NCM/PIM-1%	225	204	184	170	153	128	167
NCM/PVDF-1%	187	186	171	157	142	116	154
NCM/PIM-0.5%	206	195	180	168	154	127	164
NCM/PVDF-0.5%	192	186	172	158	140	112	157
NCM/PIM-0.1%	201	193	180	167	152	128	162
NCM/PVDF-0.1%	178	176	165	153	138	115	151

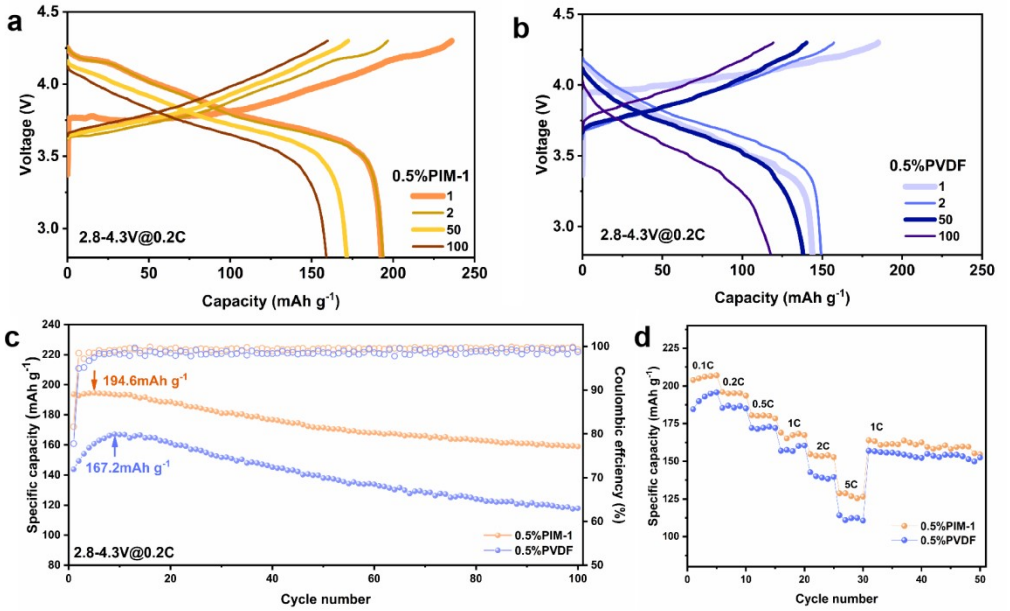

Figure S6. Charge/discharge curves of the NCM/PIM-0.5% (a) and NCM/PVDF-0.5% (b) electrodes with the voltage between 2.8 V and 4.3 V at 40 mA·g^{-1} (0.2 C, 1C=200 mA·g^{-1}) in the commercial electrolyte of 1 M $LiPF_6$ in EC/DMC (vol ratio of EC:DMC=3:7); discharge capacities over 100 cycles at 40 mA·g^{-1} (c); rate performance of the NCM/PIM-0.5% and NCM/PVDF-0.5% electrode at different current densities (d).

Regarding the PVDF containing electrodes, a reversible capacity of 118 mAh·g^{-1} with capacity retention of 70.5% is exhibited by NCM/PVDF-0.5% after 100 cycles.

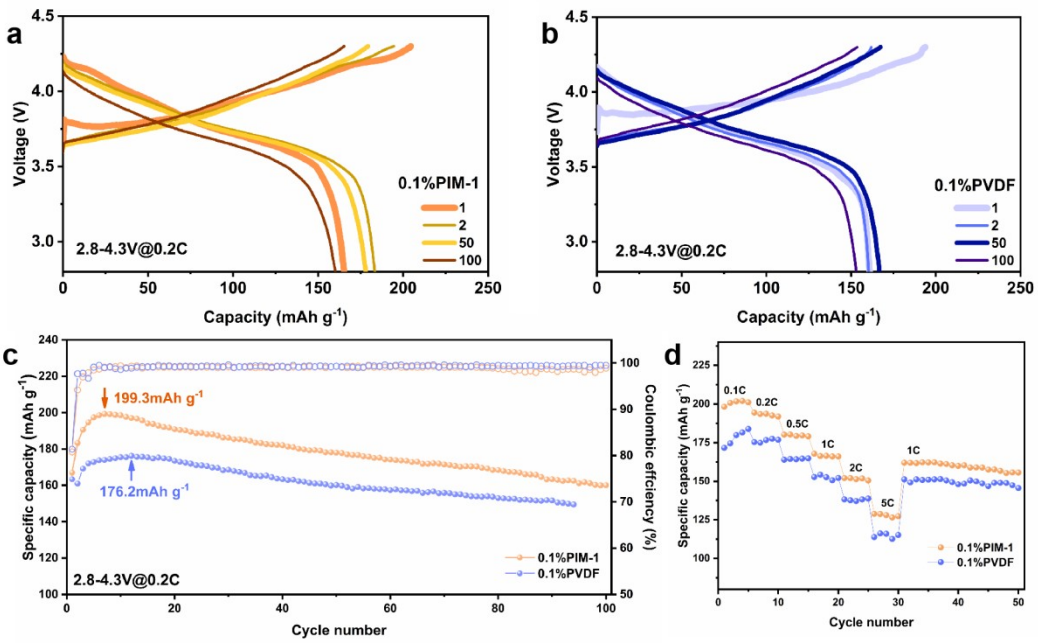

Figure S7. Charge/discharge curves of the NCM/PIM-0.1% (a) and NCM/PVDF-0.1% (b) electrodes with the voltage between 2.8 V and 4.3 V at 40 mA·g^{-1} (0.2 C, 1C=200 mA·g^{-1}) in the commercial electrolyte of 1 M $LiPF_6$ in EC/DMC (vol ratio of EC:DMC=3:7); discharge capacities over 100 cycles at 40 mA·g^{-1} (c); rate performance of the NCM/PIM-0.1% and NCM/PVDF-0.1% electrode at different current densities (d).

The NCM/PVDF-0.1% shows reversible capacity of 150 mAh·g^{-1} after 95 cycles, which collapses thereafter. The NCM/PVDF-0.1% electrode bears unstable cyclic property which hardly survives more than 100 cycles. The inferior performance of the NCM-PVDF-0.1% electrode is also reflected by the very low yield rate of electrode fabrication. It is found very difficult to form high quality electrode with good electrochemical performance using 0.1% of PVDF.

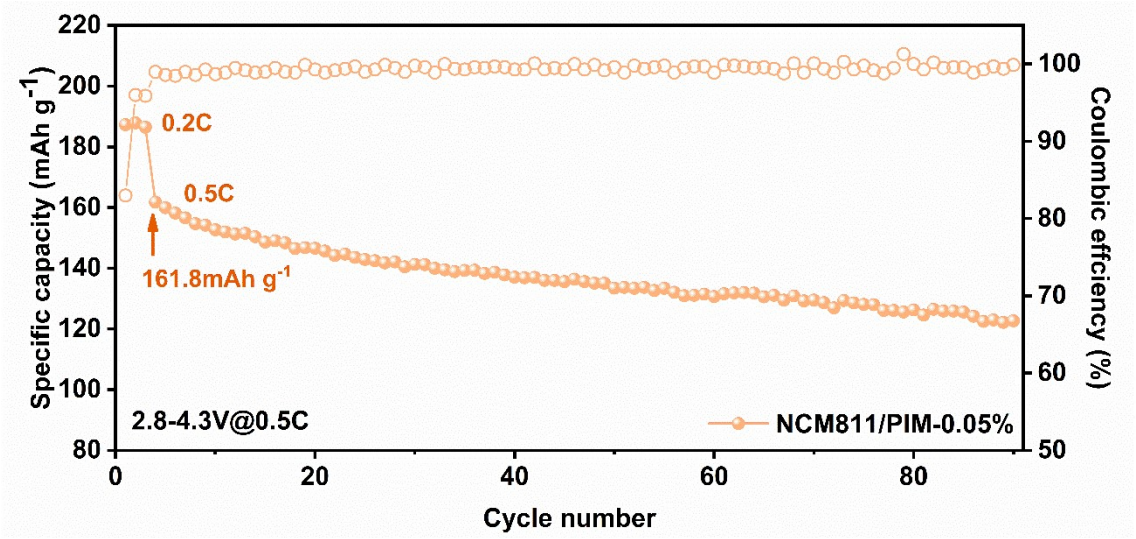

Figure S8. Cyclic performance in terms of discharge capacity and coulombic efficiency of the NCM/PIM-0.05% electrode with the voltage between 2.8 V and 4.3 V and the first three cycles at 0.2 C and following cycles at 0.5 C (1C=200 $mA \cdot g^{-1}$) in the electrolyte of 1 M $LiPF_6$ in EC/DMC (vol ratio of EC:DMC=3:7).

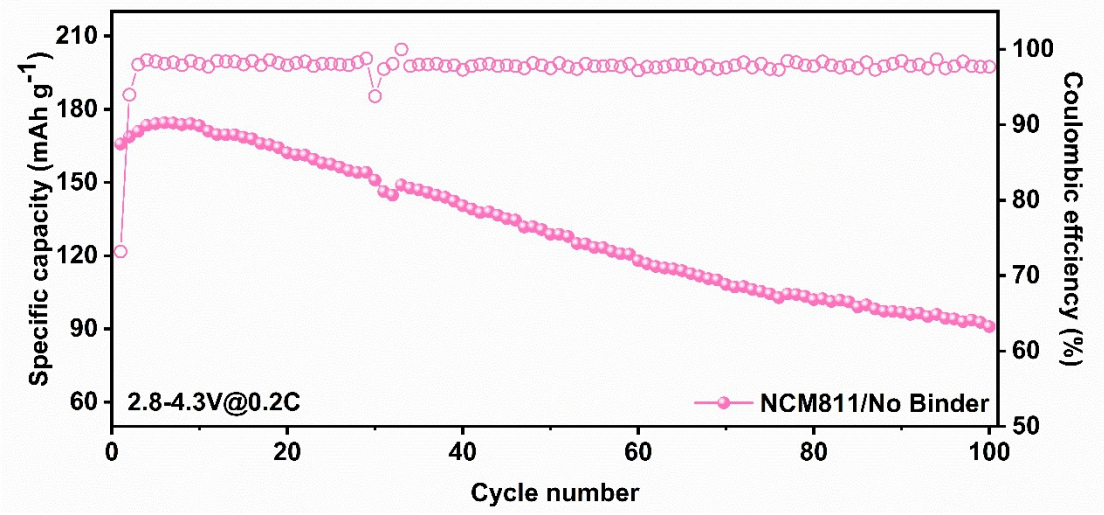

Figure S9. Cyclic performance in terms of discharge capacity and coulombic efficiency of the binder free NCM811 electrode with 90 % of NCM 811 and 10 % of super P with the voltage between 2.8 V and 4.3 V at 40 $mA \cdot g^{-1}$ (0.2 C, 1C=200 $mA \cdot g^{-1}$) in the electrolyte of 1 M $LiPF_6$ in EC/DMC (vol ratio of EC:DMC=3:7).

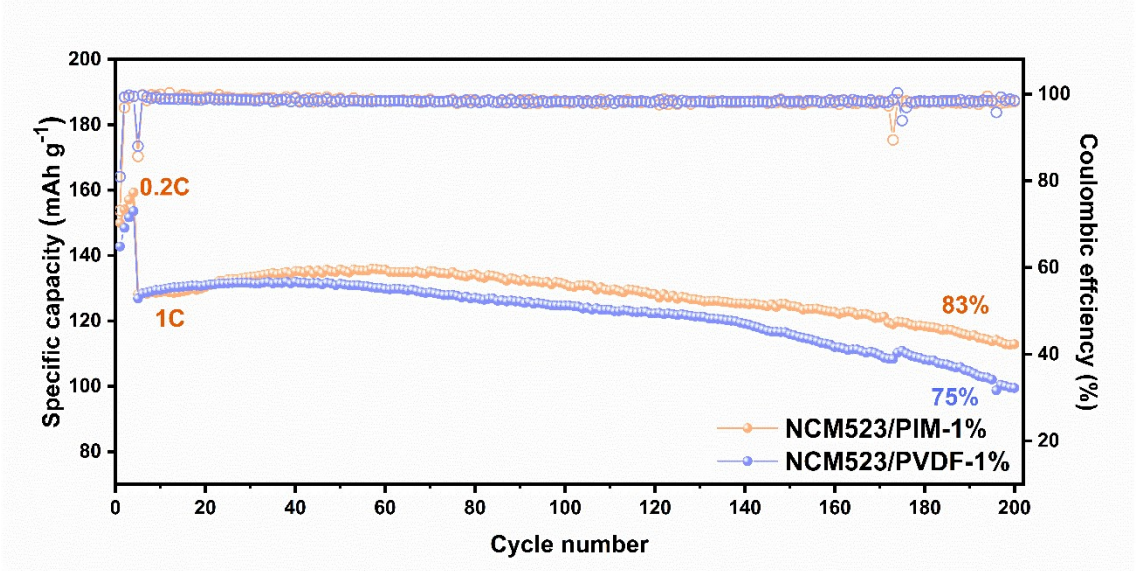

Figure S10. Cyclic performance in terms of discharge capacity and coulombic efficiency of the NCM523/PIM-1% and NCM523/PVDF-1% electrodes with the voltage range of 2.8 V-4.3 V in the electrolyte of 2 M $LiPF_6$ in EC/DMC (vol ratio of EC:DMC=3:7). The cell is activated with four cycles at 0.2 C, followed by cycles at 1 C (1C=170 $mA \cdot g^{-1}$).

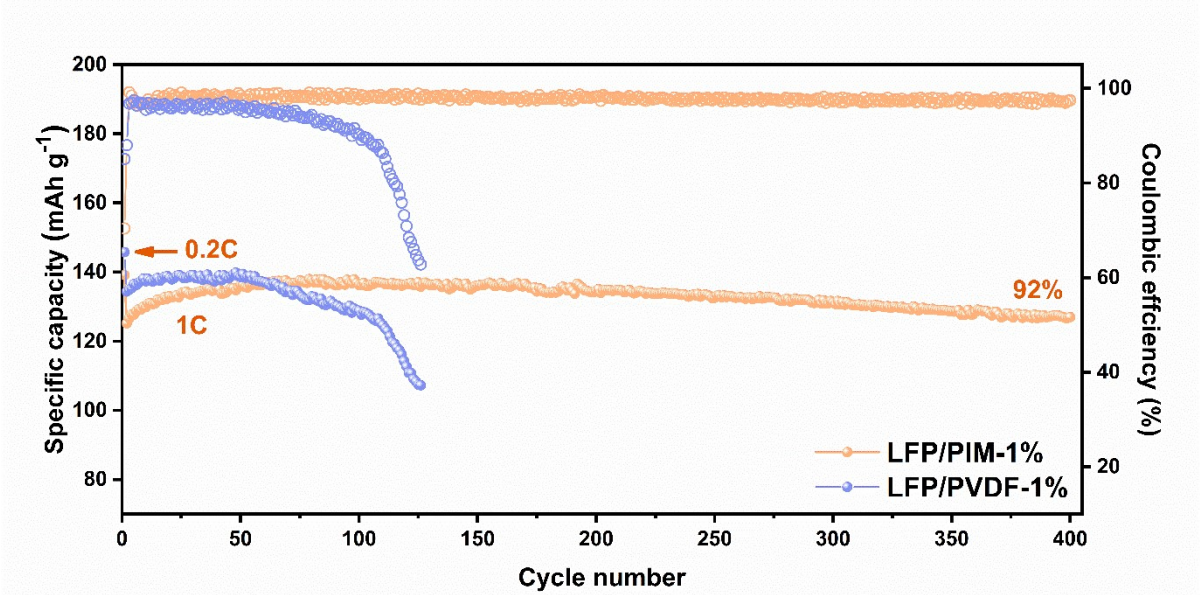

Figure S11. Cyclic performance in terms of discharge capacity and coulombic efficiency of the LFP/PIM-1% and LFP/PVDF-1% electrodes with the voltage range of 2.5 V-4.2 V in the electrolyte of 2 M $LiPF_6$ in EC/DMC (vol ratio of EC:DMC=3:7). The cell is activated with one cycle at 0.2 C, followed by cycles at 1 C (1C=170 $mA \cdot g^{-1}$).

Lower capacities are exhibited by the LFP/PIM-1% electrode than the LFP/PVDF-1% electrode in the first 50 cycles. However, the capacities continue to rise over cycles which finally surpass the capacities of the electrodes with the PVDF binder. It seems an activation process takes place during the first 50 cycles with 1% of the PIM-1 additive. It likely originates from the small particle size feature of the LFP particle, where the electrolyte wetting onto the LFP particles through the PIM-1 additive takes time to complete. Besides, side reactions between the LFP particles and nanoporous PIM-1 additive tend to be enhanced, leading to compromised coulombic efficiencies during the first 50 cycles.

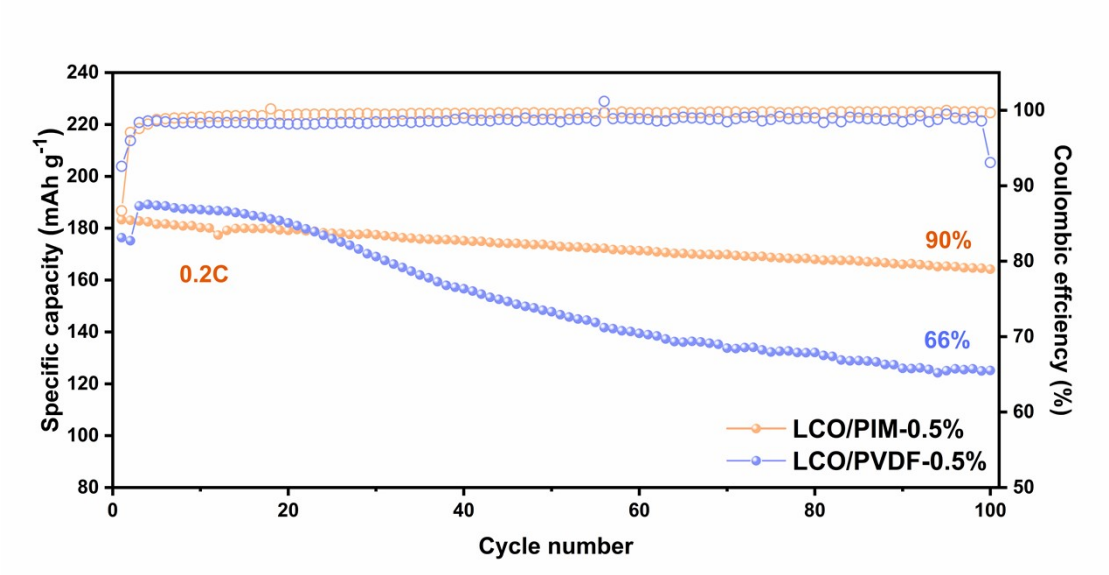

Figure S12. Cyclic performance in terms of discharge capacity and coulombic efficiency of the LCO/PIM-0.5% and LCO/PVDF-0.5% electrodes with the voltage range of 3.0 V-4.5 V at 0.2 C in the electrolyte of 1 M $LiPF_6$ in EC/DMC (vol ratio of EC:DMC=3:7) (1C=185 $mA \cdot g^{-1}$).

Concerning the LCO electrode, the LCO/PIM-0.5% electrode shows less capacity than the LCO/PVDF-0.5% electrode in the first 20 cycles, which is nevertheless stable over cycles. However, the capacity of the LCO/PVDF-0.5% electrode is gradually decreasing, which is below the capacity of the LCO/PIM-0.5% electrode after around 20 cycles. It suggests that the PIM-1 additive stabilizes the electrode despite of the lower capacities in the first 20 cycles. Firstly, the size of the LCO particles is large, which requires less amount of PVDF to cover the particle surface, leading to a good interface contact between the LCO particle and PVDF/carbon black composite. Secondly, the decreased amount of the PVDF binder (0.5%) is beneficial for the electrochemical kinetics, where the electrochemical kinetics is not compromised by the PVDF significantly. Thirdly, less volume is possessed by the PVDF binder compared

to the PIM-1 additive with the same mass composition because it is free of nanoporous structure. The reduced volume ratio helps to maintain a good charge carrier transportation at the beginning of the cycles because the region composed of the PVDF/PIM-1 component is regarded less charge carrier conductive. Based on these reasons, the LCO/PVDF electrode with 0.5% of PVDF shows higher capacities than the LCO/PIM-1 electrode in the first 20 cycles. However, continuous capacity decay takes place because the small amount of PVDF binder cannot stabilize the electrode, and suppress excessive decomposition of electrolyte effectively. It needs to point out that the NCM/PVDF electrode with 0.5% of PVDF shows less capacity than the NCM/PIM-1 electrode from the beginning of the cycles, which is different from the behavior observed in the LCO cathode system. The NCM particles utilized in this work have a smaller particle size than the LCO particles, which results in a relatively higher specific surface area. Consequently, it becomes challenging for the PVDF/carbon black composite to form a good coating layer on the surface of the NCM particles, leading to a deteriorated electrochemical kinetics. Therefore, it is reasonable to expect that the NCM/PVDF electrode shows worse performance than the LCO/PVDF electrode in terms of electrochemical kinetics with the same mass composition of 0.5%.

Table S2. Fitting Data of the EIS of the NCM/PIM-1% and NCM/PVDF-1% electrodes after representative cycles.

Cycle		1	5	10	50	100	1	5	10	50	100
Sample		R_{CEI}/Ohm					R_{CT}/Ohm				
1%	PIM-1	81.06	12.50	5.35	1.62	1.34	358.7	246.9	186.7	545.2	783
	PVDF	72.24	22.13	16.74	2.50	2.33	818.8	453.3	589.3	765.7	896.1

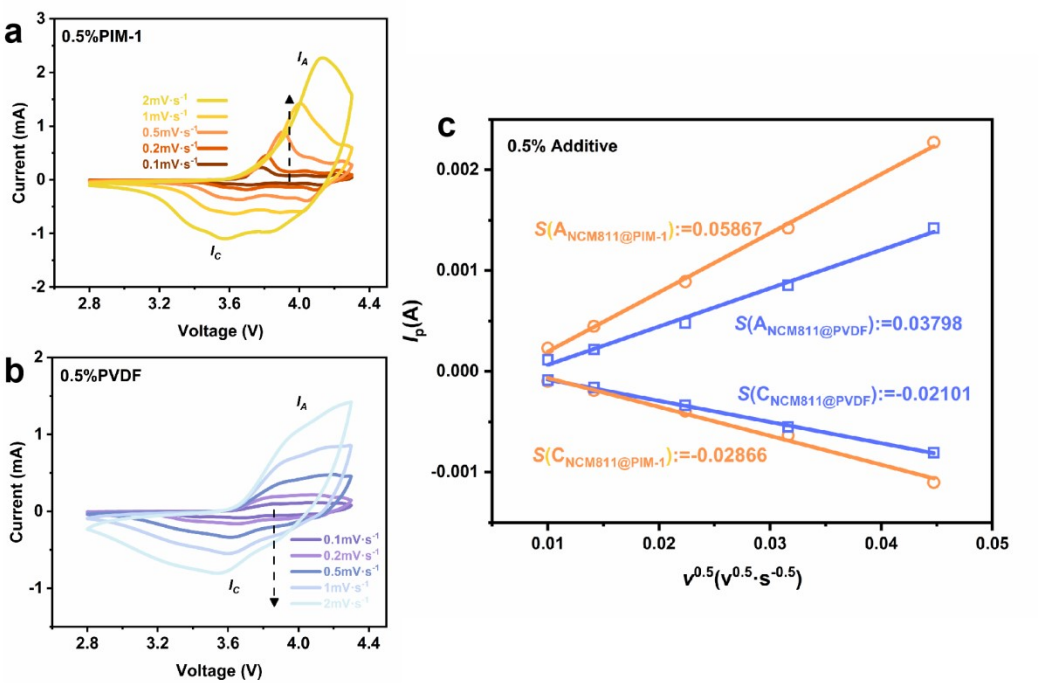

Figure S13. Cyclic voltammetry (CV) curves of the NCM/PIM-0.5% (a) and NCM/PVDF-0.5% (b) electrodes at different scan rates. c) Linear fits for the cathodic and anodic peak currents versus square root of the scanning rates of NCM/PIM-0.5% (orange) and NCM/PVDF-0.5% (blue) derived from (a) and (b).

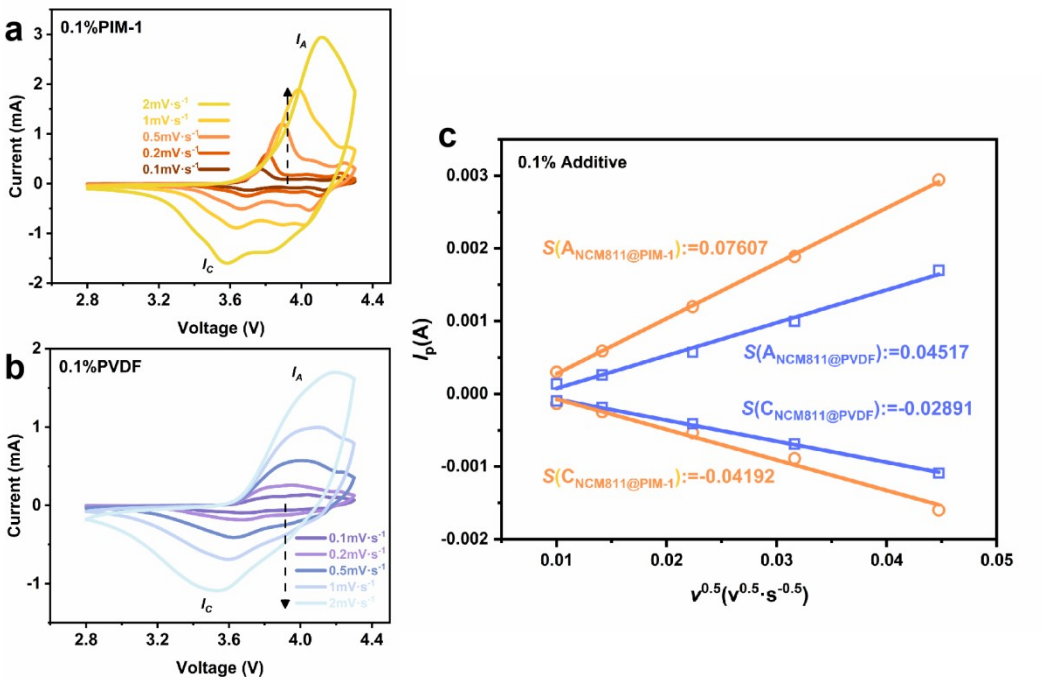

Figure S14. Cyclic voltammetry (CV) curves of the NCM/PIM-0.1% (a) and NCM/PVDF-0.1% (b) electrodes at different scan rates. c) Linear fits for the cathodic and anodic peak currents versus square root of the scanning rates of NCM/PIM-0.1% (orange) and NCM/PVDF-0.1% (blue) derived from (a) and (b).

The Li-ion diffusion coefficients of the NCM/PIM and NCM/PVDF electrodes with different compositions of PIM and PVDF (1%, 0.5%, and 0.1%) are calculated according to the classical Randles–Sevcik equation (Equation (2)):

$$Ip=2.69\times10^{5}n^{1.5}AD_{Li}{}^{+0.5}v^{0.5}C_{Li}{}^{+} \quad (2)$$

where Ip indicates the peak current representing the number of electrons in the reaction; A is the electrode area (cm^2); $D_{Li}{}^{+}$ is the Li-ion diffusion coefficient ($cm^2 \cdot s^{-1}$); v is the scanning rate ($V \cdot s^{-1}$) and $C_{Li}{}^{+}$ is the Li-ion concentration in the electrolyte ($mol \cdot cm^{-3}$).

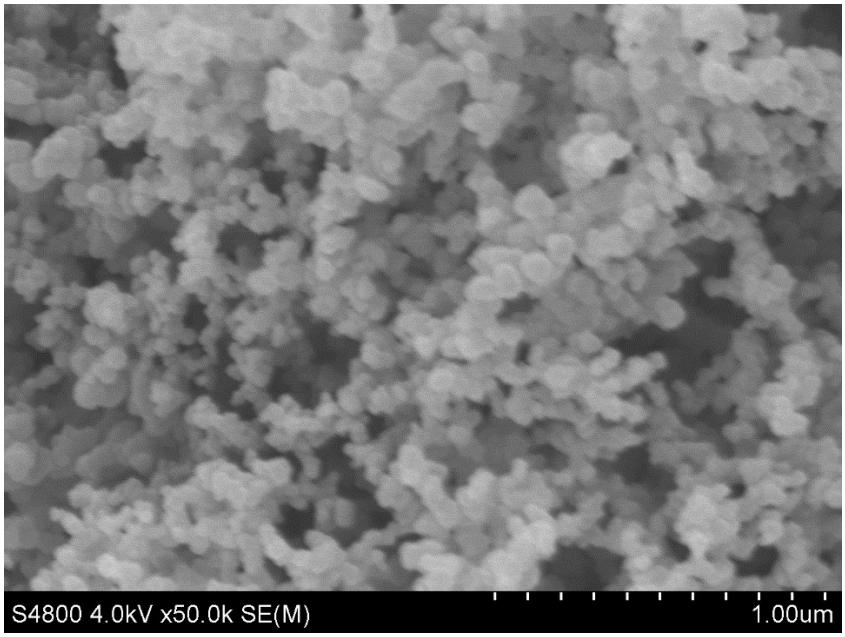

Figure S15. Morphology of conductive carbon black (Super P) by SEM.

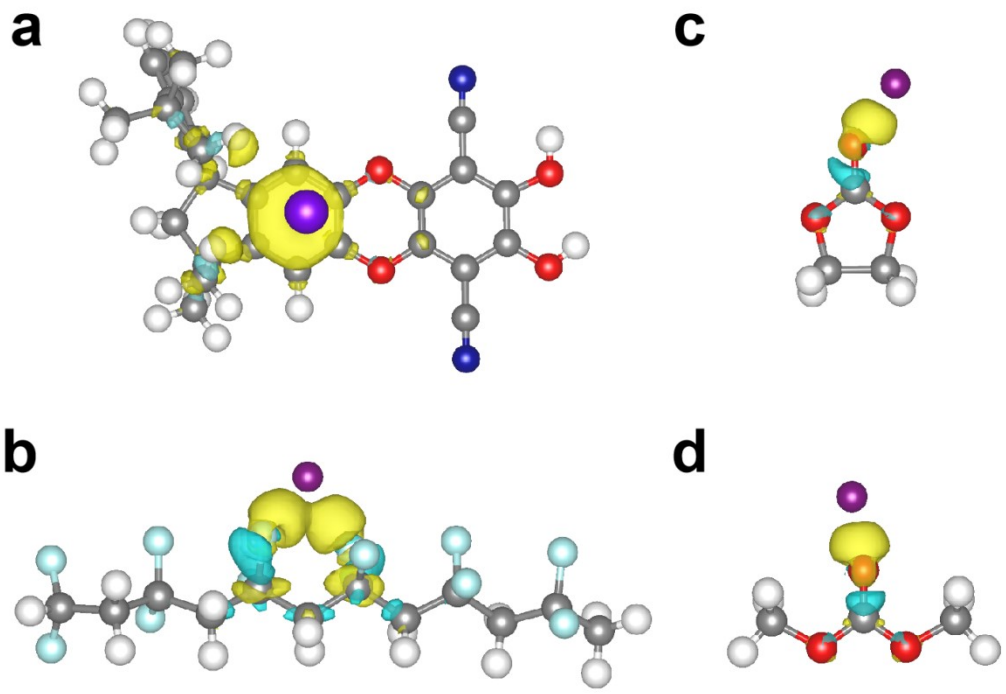

Figure S16. Charge density difference of PIM (a), PVDF (b), EC (c), and DMC (d) adsorbing Li^+ (yellow is the increase in electron density, blue is the decrease in electron density) in electrolyte solvent (EC: DMC=3:7).

Table S3. Mass Loading Density of the Electrodes with respect to the Active Material

Testing condition	Mass loading density of the electrodes mg·cm^{-2}					
	NCM/PIM -1%	**NCM/PIM -0.5%**	**NCM/PIM -0.1%**	**NCM/PVDF -1%**	**NCM/PVDF -0.5%**	**NCM/PVDF -0.1%**
Cycling	4.21	4.39	3.72	3.87	4.81	5.33
Rate	5.17	4.82	4.31	4.57	5.42	5.26

References

1. Pan, Y.; Zhai, X.; Yin, J.; Zhang, T.; Ma, L.; Zhou, Y.; Zhang, Y.; Meng, J., *ChemSusChem* **2019,** *12* (10), 2231-2239.
2. Ma, L.; Meng, J.; Pan, Y.; Cheng, Y. J.; Ji, Q.; Zuo, X.; Wang, X.; Zhu, J.; Xia, Y., *Langmuir* **2020,** *36* (8), 2003-2011.
3. Stefan, G.; Jens, A.; Stephan, E.; Helge, K., *The Journal of Chemical Physics* **2010**.
4. Vincenzo, B.; Maurizio, C.; Jacopo, T., *Journal of Computational Chemistry* **1998**.
5. Lu, T.; Chen, F., *Journal of Computational Chemistry* **2012,** *33* (5), 580-592.
6. Humphrey, W.; Dalke, A.; Schulten, K., *Journal of Molecular Graphics & Modelling* **1996,** *14* (1), 33-38.
7. Sun, H., *Journal of Physical Chemistry B* **1998,** *102* (38), 7338-7364.
8. Ma, Y.; Liu, Y.; Yu, T.; Lai, W.; Ge, Z.; Jiang, Z., *Propellants Explosives Pyrotechnics* **2018,** *43* (2), 170-176.